Global and Planetary Change 246 (2025) 104719

Contents lists available at ScienceDirect

Global and Planetary Change

journal homepage: www.elsevier.com/locate/gloplacha

Spatiotemporal variation of dissolved rare earth elements in the North Pacific Subtropical Gyre: Influence of biogeochemical cycling and application in tracing deep water

Axiang Cao [a,b], Qian Liu [a,*], Jing Zhang [a,c], Zhensong Liu [a,b], Jingling Ren [a,d], Yihua Cai [e], Kuanbo Zhou [e], Xianghui Guo [e], Xin Liu [e]

[a] Frontiers Science Center for Deep Ocean Multispheres and Earth System, and Key Laboratory of Marine Chemistry Theory and Technology, Ministry of Education, Ocean University of China, Qingdao 266100, China
[b] College of Chemistry and Chemical Engineering, Ocean University of China, Qingdao 266100, China
[c] Faculty of Science, Academic Assembly, University of Toyama, Toyama 9308555, Japan
[d] Laboratory for Marine Ecology and Environmental Science, Qingdao National Laboratory for Marine Science and Technology, Qingdao, China
[e] State Key Laboratory of Marine Environmental Science and College of Ocean and Earth Sciences, Xiamen University, Xiamen 361000, China

ARTICLE INFO

Editor: Dr Sun Jimin

Keywords:
NPSG
Rare earth elements
Seasonal variation
Biogeochemical cycling
Ocean interfaces
Water mass tracing

ABSTRACT

The North Pacific Subtropical Gyre (NPSG), the largest continuous marine ecosystem, significantly influences the cycling of trace elements through biological and seawater interface processes. Understanding these processes, particularly their seasonal impacts, is crucial for tracing oceanic dynamics, yet remains underexplored. In this context, rare earth elements (REEs) in seawater serve as valuable tracers for studying these processes. This study presents the spatiotemporal distribution of dissolved REE concentrations based on two GEOTRACES-CHINA process study cruises (GPpr15) conducted in summer and winter, along with published results from a GEOTRACES-CHINA cruise (GP09) during spring. Above the depth of chlorophyll maxima (DCM), REE levels were lowest in winter compared to summer, reflecting enhanced scavenging of REEs by particulate matter, primarily driven by increased chlorophyll-α during winter. In subsurface to intermediate waters (150–1000 m), release efficiencies (~0.04 pmol Nd/μmol apparent oxygen utilization) exhibited no seasonal variations in the NPSG. These efficiencies were consistent with those in the North Atlantic Gyre at similar latitudes, but differed from those at higher latitudes (~0.15), which may be attributed to variations in the plankton community structure across regions. Furthermore, inputs of slope sediments to intermediate waters (500–1000 m) off the Philippine Islands were identified using Ce anomalies and Yb/Nd ratios. These inputs peaked during winter, with Nd contribution from slope sediment accounting for 15–43 % of the total Nd concentration. In deep waters (>4500 m) of the Philippine Basin (stations K2/K2b, K3, K13/13a, and K14), elevated REE concentrations indicated extra inputs from the seafloor and lateral transport from the Philippine Islands, contributing 17 ± 6 % of Nd. The contributions of Nd from settled particles and water mass mixing were estimated at 10 ± 5 % and 73 ± 3 %, respectively. Additionally, Yb reliably traced the distribution of lower circumpolar deep water in the Philippine Basin. In summary, these findings highlight the significant influence of biogeochemical processes on seasonal variations of REEs above the DCM and underscore the potential of REE in tracking deep water transport.

1. Introduction

The subtropical gyre represents the largest continuous ecosystem on Earth (Karl, 1999). Among these gyres, the North Pacific Subtropical Gyre (NPSG) is the most extensive oligotrophic region (Dai et al., 2023), making it a key area for exploring trace element biogeochemical processes. Rare earth elements (REEs), a chemically coherent group of 14 elements, are typically categorized into light REEs (LREEs; La, Ce, Pr, and Nd), middle REEs (MREEs; Sm, Eu, Gd, Tb, and Dy) and heavy REEs (HREEs; Ho, Er, Tm, Yb, and Lu) based on atomic mass. The ionic radius and chemical properties of yttrium (Y) closely resemble those of Ho, an HREE, and therefore Y is classified as one of the REEs (Shannon, 1976).

* Corresponding author.
E-mail address: liuqian@ouc.edu.cn (Q. Liu).

https://doi.org/10.1016/j.gloplacha.2025.104719
Received 30 August 2024; Received in revised form 18 January 2025; Accepted 18 January 2025
Available online 21 January 2025

Their coherent chemical properties and systematic changes make REEs valuable as tracers for oceanographic processes, such as atmospheric deposition, riverine and sediment inputs (e.g., Zhang et al., 2008; Fröllje et al., 2016; Behrens et al., 2018; Cao et al., 2024), and the mixing of water masses (Zhang et al., 2018; Garcia-Solsona et al., 2020; Seo and Kim, 2020; Liu et al., 2022; Cao et al., 2023). Systematic variations in the chemical behavior of REEs are governed by their interactions with particulate matter. In seawater, trivalent REEs predominantly form carbonate complexes, while HREEs exhibit a stronger affinity for inorganic complexes (Goldberg et al., 1963; Cantrell and Byrne, 1987), contributing to their enhanced stability and retention in the seawater. In contrast, LREEs are more readily adsorbed onto organic ligands on particle surfaces, leading to their preferential removal from seawater. This behavior results in the characteristic PAAS-normalized seawater REE pattern of HREE enrichment relative to LREE (e.g., Elderfield and Greaves, 1982; Bertram and Elderfield, 1993; Alibo and Nozaki, 1999). Ce exhibits a different oxidation state in seawater from other LREEs, as dissolved Ce^{3+} tends to oxidize to particulate Ce (IV), leading to its removal from the water column and a corresponding negative Ce anomaly in normalized REE patterns (de Baar et al., 1988; Schijf et al., 1991; Tazoe et al., 2011).

Seasonal variations in REE concentrations have been documented in surface waters at Station ALOHA, likely due to atmospheric and riverine inputs (Fröllje et al., 2016). However, in areas further removed from terrestrial influences, biogeochemical processes within seawater may exert a more pronounced effect on REE distributions. For example, in shallow waters, REEs are readily scavenged by particulate matter, resulting in reduced concentrations. At greater depths, microbial-mediated decomposition of sinking organic matter facilitates the release of REEs into the water column, a process referred to as remineralization (Stichel et al., 2015; Lambelet et al., 2016; Behrens et al., 2018; Cao et al., 2023, 2024). Nonetheless, the influence of temporal variations in biogeochemical processes on REE distributions remains poorly understood. This gap in knowledge regarding the role of REEs as tracers in oceanic may lead to an incomplete understanding of the marine processes.

The mass balance of dissolved REEs in the oceans remains inadequately constrained (Tachikawa, 2003; Johannesson and Burdige, 2007). There are two main mechanisms contributing to the sources of dissolved REEs in the ocean: (1) a "top-down" driven model, which primarily refers to the input of REEs through riverine and eolian processes (Siddall et al., 2008), and (2) a "bottom-up" benthic source model, where REEs are released from pore water in sediment into the bottom waters (Abbott et al., 2015a, 2015b; Haley et al., 2017). While significant benthic fluxes of REEs have been revealed in multiple settings, the bottom-up mechanism does not apply to all regions, for example in the Bay of Bengal (Yu et al., 2017a, 2017b). This may be related to the deep-water environment and the rate of sediment accumulation, which still needs further study. Understanding the interplay between these mechanisms and their regional variability is essential for a more comprehensive understanding of REE cycling in seawater. Thus, clarifying and quantifying these sources is essential for refining the global oceanic REE budget.

The deep water circulation in the North Pacific is pivotal for understanding global climate change (Johnson et al., 2007). Despite its importance, the flow path of the Lower Circumpolar Deep Water (LCDW) in the Philippine Sea remains sparsely documented. Tian et al. (2021) employed historical hydrographic data to investigate the pathway of LCDW in this region. However, given the complex seafloor topography of the Philippine Sea, additional evidence on the LCDW distribution is necessary. Furthermore, the temporal trends of the potential temperature of deep water exhibit high uncertainty. Studies based on in situ observations, reanalysis data, and historical records have reported divergent trends, with some indicating a cooling trend in Pacific abyssal waters (Wunsch and Heimbach, 2014; Gebbie and Huybers, 2019), and others suggesting a warming trend (Johnson et al., 2007; Tian et al., 2021). Consequently, relying solely on potential temperature and salinity to identify the deep water masses may introduce potential biases. Future advancements in understanding the mixing of deep water masses could benefit from integrating thermohaline properties with chemical tracers. HREE, such as Yb, is predominantly controlled by the water masses mixing in the Northwest Pacific (>93 ± 4 %, Cao et al., 2024), and thus, its distribution could provide valuable insights into the transport of deep water masses in the Philippine Sea.

This study aims to elucidate the seasonal variation of biological processes and seawater interface processes affecting the cycling of REE, using data collected from two GEOTRACES cruises conducted during the summer and winter, along with published results from a GEOTRACES-CHINA cruise (GP09) during the spring in the NPSG. We observed seasonal variations in REE concentrations above the depth of chlorophyll maxima (DCM). Below the DCM, we identified spatial variability and seasonal stability in REE release efficiency from remineralization processes and revealed the potential implications of the consistent Nd to apparent oxygen utilization (AOU) ratios. Additionally, at the seawater interface, we estimated the contributions from slope sediment inputs in the intermediate water and excess particles in the deep waters to REE concentrations at the stations near the Philippine Islands. In deep water, the pathway of the LCDW from the Pacific into the Philippine Sea was effectively traced using Yb.

2. Materials and methods

2.1. Study area

The NPSG is bounded by several major ocean currents, including the Kuroshio Extension Current, the California Current, the North Equatorial Current (NEC), and the Kuroshio Current (Dai et al., 2023).

The North Pacific Tropical Surface Water (NPTSW), situated at a shallow depth of approximately 100 m, is characterized by high temperatures and low salinity, a result of precipitation exceeding evaporation in the tropical North Pacific (Sun et al., 2008). Beneath the NPTSW lies the North Pacific Tropical Water (NPTW), which exhibits a subsurface salinity maximum. This water mass forms through the subduction of subtropical surface waters in the gyre center, where evaporation surpasses precipitation, with a core distribution centered at 10–23°N in the study area (Tsuchiya, 1968; Suga and Kato, 2000). The Subtropical Mode Water (STMW), generated in a deep winter mixing layer south of the Kuroshio Current and Kuroshio Extension Current, extends from 132°E to near the dateline. It is distinguished by nearly uniform potential temperature and salinity throughout its vertical profile (Oka and Qiu, 2012). In the intermediate water layer, the North Pacific Intermediate Water (NPIW) and modified Antarctic Intermediate Water (modified AAIW) predominate. The modified AAIW originates from the mixing of AAIW with upwelled Pacific Deep Water (Bostock et al., 2013). The NPIW dominates north of 15°N, whereas the modified AAIW prevails to the south of this latitude (Cao et al., 2024).

At depth, the Circumpolar Deep Water (CDW), formed in the Antarctic, bifurcates into Upper CDW (UCDW) and Lower CDW (LCDW) during its northward transport, with a vertical division at a potential temperature of 1.2 °C in the western Pacific (Johnson and Toole, 1993; Johnson et al., 1994; Tian et al., 2021; Wang et al., 2023). The UCDW reaches the Philippine Sea at depths of 2000–2500 m, upwelling at around 2000 m (Kawabe et al., 2003, 2009; Kawabe and Fujio, 2010). The North Pacific Deep Water (NPDW), the oldest deep water mass, is characterized by low oxygen content and marked by a high-silicate tongue at depths of 2500–3500 m (Talley et al., 2011; Siedler and Müller, 2004). Compared to the NPDW, the LCDW is both colder and saltier.

2.2. Sample collection and ancillary data

During two GEOTRACES-CHINA process study cruises GPpr15-

summer (KK2003, 3 July–20 August 2020) and GPpr15-winter (KK2007, 23 December 2020–7 February 2021), seawater samples were collected from 23 stations within the NPSG aboard the R/V TAN KAH KEE (Fig. 1). Vertical sampling was conducted across 14 to 48 layers, yielding a total of 542 samples. Eight stations were sampled seasonally and divided into two distinct transects: the 11°N transect, which included stations K8a, K9a, K11a, K12a, and K13a/K13; and the 155°E transect, which included stations M18, M22, and M30. During the cruises, seawater samples were collected from 12 L Teflon-lined Niskin-X bottles mounted on an epoxy-coated conductivity-temperature-depth (CTD, Sea-Bird 911 plus) sensors frame. The collected water was promptly transferred to an onboard class-1000 clean laboratory, where it was filtered through Pall AcroPak 1000 cartridge filters (0.45 μm pore size) into 500 mL Low-Density Polyethylene bottles (Nalgene, Thermo Fisher Scientific). The filtrate was then acidified to a pH of ≤2 using 6 M ultra-pure hydrochloric acid (Optima grade, Fisher Chemical).

The SBE 911plus CTD sensor was utilized to obtain data on salinity and temperature, while dissolved oxygen (DO) levels were measured by Winkler spectrophotometry (Labasque et al., 2004) at specific depths. Chlorophyll-α concentrations were determined with a Turner Designs fluorometer, following the protocol established by Welschmeyer (1994).

2.3. Rare earth elements analysis

In a class 1000 cleanroom, 150–180 mL of seawater was concentrated using NOBIAS PA1 (Takata et al., 2009) and analyzed by an inductively coupled plasma-mass spectrometer (ICP-MS, Thermo iCAP Q). After the concentration process with Milli-Q water (Millipore), REE determinations were performed to assess the procedure blank and calculate the standard deviation (SD). The limit of detection (LOD) was defined as three times the standard deviation (3SD). The relative standard deviations (1σ RSD) of repeated REE measurements in Pacific surface waters ($n = 4$) and deep waters (4000 m, $n = 11$) were both below 5 %. The average procedure blank ($n = 20$) accounted for less than 3 % of the REE concentrations in surface water (n = 4), which are among the lowest concentrations recorded in the ocean. La was an exception, with a blank contribution of 4.1 %. The concentration of Ce in deep water is typically low, with blank values representing less than 3 % of the measured Ce concentration in seawater at 4000 m depth (n = 11). Further details are provided in Supplementary Table S1.

The external consistency of the data was evaluated using the certified reference material NASS-7 (Seawater; from the National Research Council of Canada), with the measurement results provided in Supplementary Table S2. Mean concentrations and associated errors were calculated from the published NASS-7 dataset (Ebeling et al., 2022; Schmidt et al., 2022; Liao et al., 2023; Kraemer et al., 2024), with deviations representing the differences between the data from this study and the published mean values. Our results are consistent with the mean values within one standard deviation (1σ RSD), confirming the reliability of the measurement in this study. Additionally, an international intercalibration of REE data was performed with the University of Southern Mississippi during the GP09 GEOTRACES cruise. The agreement between the datasets confirms the reliability of our REE data. Additional details regarding the intercalibration methodology and results are available in Cao et al. (2024).

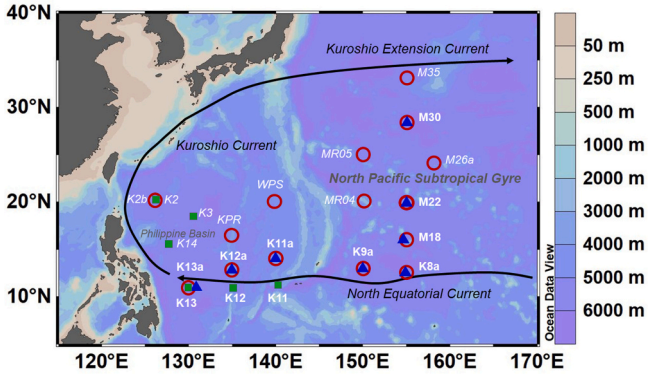

Fig. 1. Location map. Sampling stations during cruise GPpr15-summer (red circles) and GPpr15-winter (blue triangles) together with the published station (green squares) from Cao et al. (2024). Station K13-K8a: transect 11°N; Station M18–30: transect 155°E. Schematic flow patterns of major surface currents are shown with black solid arrows. Maps were created using Ocean Data View (ODV) software (Schlitzer, 2016). (For interpretation of the references to colour in this figure legend, the reader is referred to the web version of this article.)

3. Results

3.1. Hydrographic setting

Fig. 2 illustrates the hydrographic characteristics of the study area, with detailed data provided in Supplementary Tables S3 and S4. The potential temperature of seawater in the region ranges from 1.00 °C to 28.89 °C in summer and from 0.97 °C to 30.04 °C in winter. The highest potential temperatures were observed in surface waters, which exhibited a moderate increase in summer compared to winter and a decline with increasing depth. In intermediate water, the potential temperature decreases below 10 °C. At depths of 4000 m, the potential temperature falls to 1.2 °C at all stations except station K13/13a, where 1.2 °C represents the upper interfaces of the LCDW. Salinities values ranged from 33.88 to 35.24 in summer and from 33.81 to 35.51 in winter. Vertically, the extreme salinities align with the characteristics of the NPTW core, which exhibits maximum salinity, and the NPIW core, which shows minimum salinity. In the deep water, specifically between 2000 m and 6000 m, salinity remains relatively stable, varying only from 34.6 to 34.7. Spatially, in association with latitude, evaporation, and precipitation, surface waters along the 11°N transect exhibited higher potential temperatures and lower salinity, whereas those along the 155°E transect displayed lower potential temperatures and higher salinity.

3.2. REE concentrations

The representativeness of a single LREE (or HREE) for all LREEs (or HREEs) has been demonstrated in the Northwest Pacific (Cao et al., 2023, 2024). Therefore, only the results for Nd (representing LREEs, except Ce) and Yb (representing HREEs) are presented (Figs. 3 and 4). The geochemical behavior of Ce differs from that of the other trivalent REEs, and it will be discussed separately.

In the study area, Nd concentrations ranged from 3.7 to 47.6 pmol/kg in summer and from 3.8 to 38.0 pmol/kg in winter, while Yb concentrations varied between 0.9 and 13.6 pmol/kg in summer and between 0.7 and 10.8 pmol/kg in winter (Supplementary Tables S3 and S4). Spatially, the vertical distribution of REE exhibited a nutrient-like pattern, with the lowest concentrations observed above the DCM (<~150 m) and concentrations gradually increasing with depth. REE concentrations were slightly higher in deep water (4500 m–6000 m) at the northern stations M35 and M30, and stations K13/13a and K2b near the Philippines compared to other stations (Figs. 3 and 4). The elevated REE concentrations (44.2 ± 2.3 pmol/kg for Nd and 11.3 ± 1.6 pmol/kg for Yb) observed in deep water (4500–5150 m) at station M35 likely result from the influence of NPDW and possible contributions from seamounts. However, further evidence is required. The concentrations of Nd and Yb were 36.6 ± 1.3 pmol/kg and 9.9 ± 0.3 pmol/kg, respectively, between 4500 m and 6000 m at stations K2b, K13/13a and M30.

Seasonally, in the seasonal sampling sites (Supplementary Table S3), during summer, Nd and Yb concentrations above the DCM ranged from 3.7 to 11.7 pmol/kg and 0.9 to 1.7 pmol/kg, respectively. In winter, these concentrations ranged from 3.8 to 6.7 pmol/kg and 0.7 to 1.6 pmol/kg, respectively. A significant seasonal variation in REE

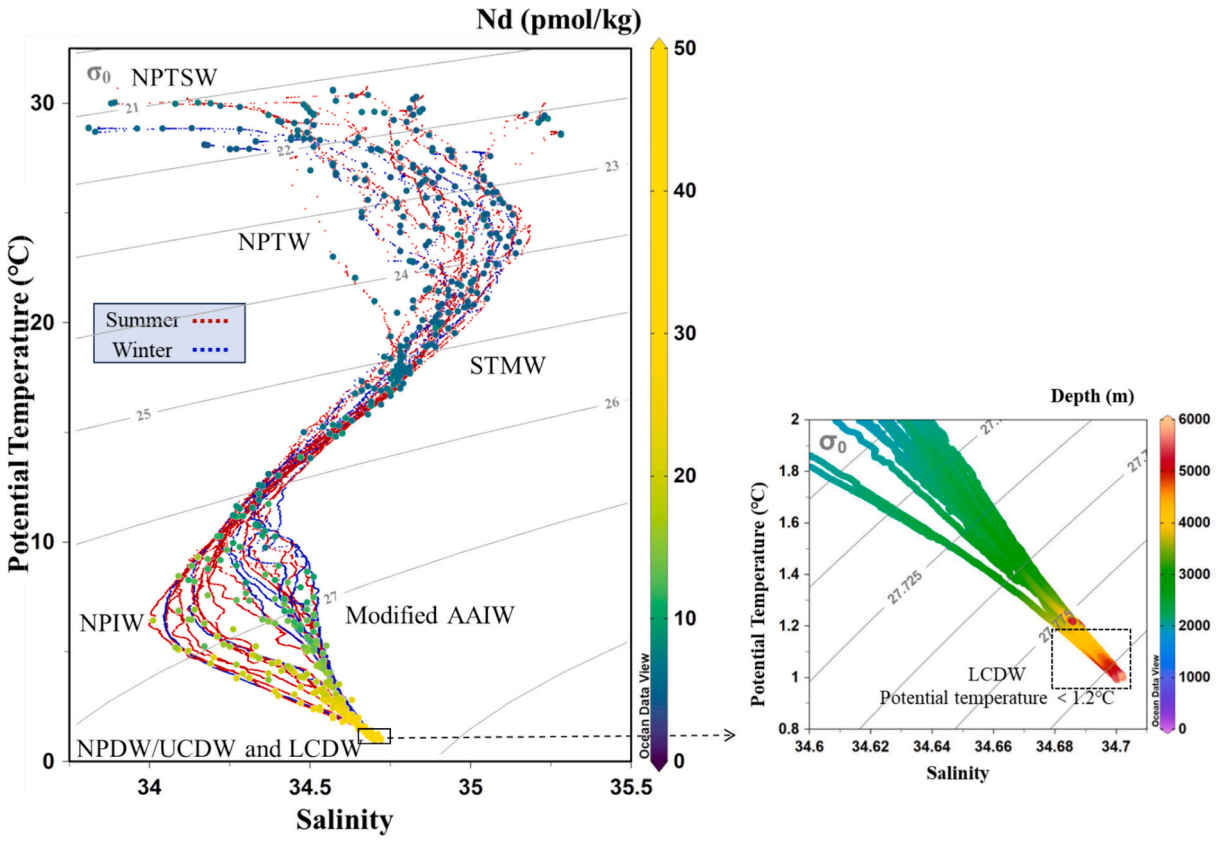

Fig. 2. (a) Potential temperature (°C)-salinity diagram from the GPpr15 cruises conducted in both summer (red dotted lines) and winter (blue dotted lines). The major identified water masses include NPTSW: North Pacific Tropical Surface Water, NPTW: North Pacific Tropical Water, STMW: Subtropical Mode Water, NPIW: North Pacific Intermediate Water, modified AAIW: modified Antarctic Intermediate Water, NPDW: North Pacific Deep Water, UCDW: Upper Circumpolar Deep Water, and LCDW: Lower Circumpolar Deep Water. Sampling sites are marked with circles, with colors representing Nd concentrations (pmol/kg). (b) Potential temperature (°C) vs. salinity diagram, with depth (m) indicated by colors. (For interpretation of the references to colour in this figure legend, the reader is referred to the web version of this article.)

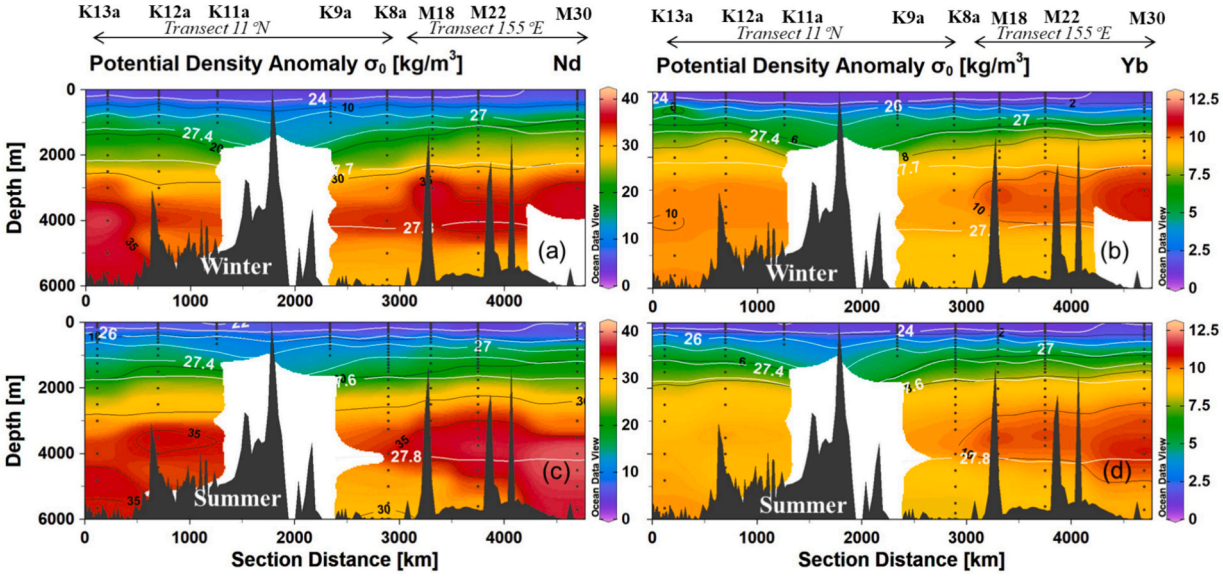

Fig. 3. Distributions of Nd (pmol/kg) and Yb (pmol/kg) with colour bars and black contours along the transects 11°N and 155°E in both winter (a and b) and summer (c and d). White contours represent potential density (kg/m^3). The transect 11°N includes stations K18-K13/13a and the transect 155°E includes stations M18, M22, and M30.

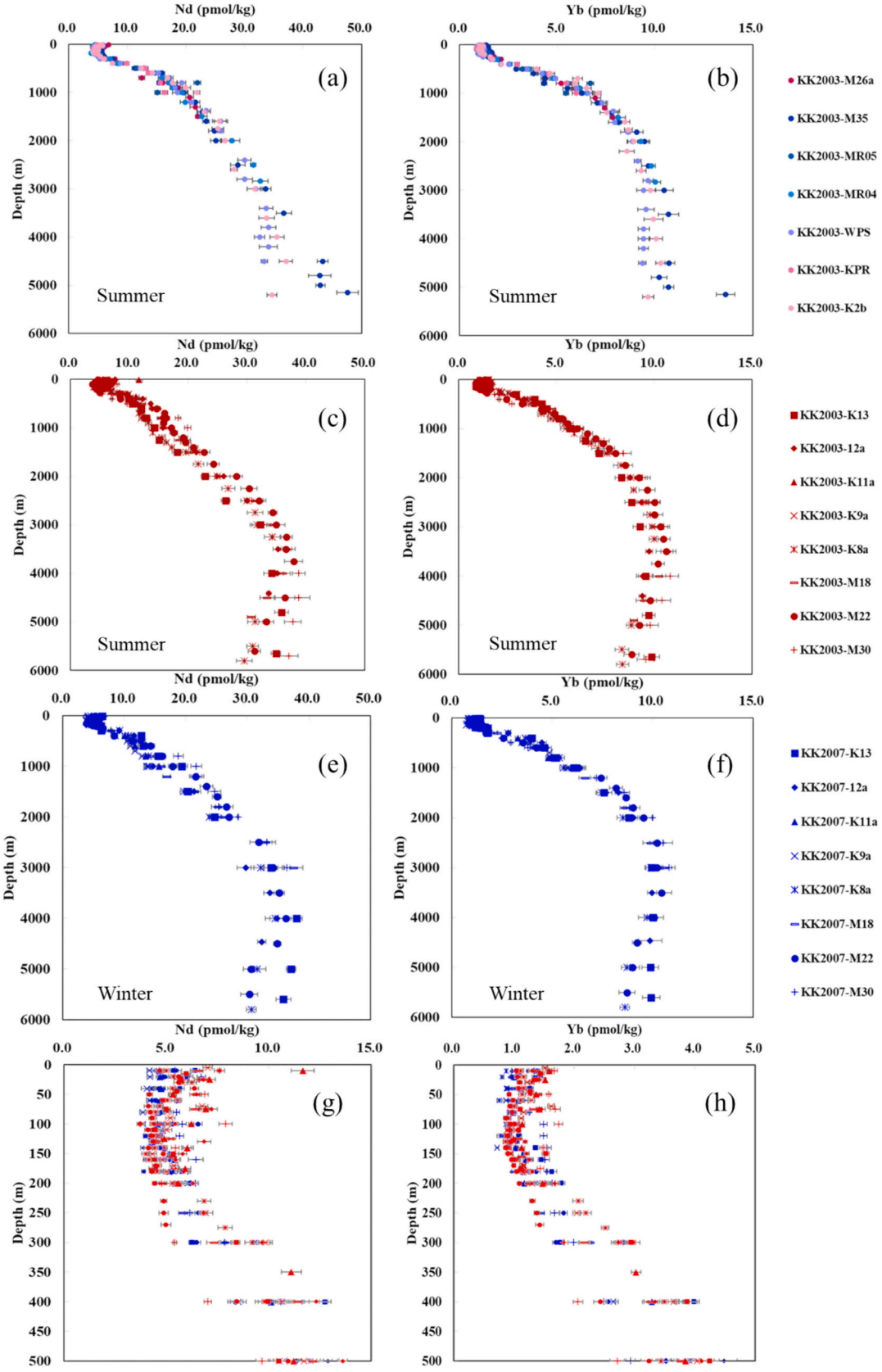

Fig. 4. Vertical profiles of Nd (pmol/kg) and Yb (pmol/kg) across the full water column for both summer (a, b, c, d) and winter (e, f). Seasonal sampling stations are shown in panels (c), (d), (e), and (f). Seasonal comparisons of Nd and Yb concentrations at depths as shallow as 500 m are presented in panels (g) and (h).

concentrations above the DCM was observed (*t*-test, $p < 0.05$), with concentrations being 3 % ~ 26 % higher in summer compared to winter. Although no statistically significant seasonal differences were observed in the subsurface/intermediate water (200–1000 m) and deep water (1000 m to the bottom) (t-test, $p > 0.05$), the Nd concentration in the intermediate water (400–1000 m) at station K13 was approximately 30 % higher in winter (15.2 ± 3.1 pmol/kg) compared to both summer (11.9 ± 1.8 pmol/kg) and spring (11.8 ± 1.1 pmol/kg) (data from Cao et al., 2024).

Unlike other trivalent REEs, Ce exists as a tetravalent ion in seawater and is readily removed through oxidation, leading to a negative anomaly relative to neighboring elements, known as the Ce anomaly (de Baar et al., 1988, 2018). The Ce anomaly (Ce/Ce*) is calculated using the formula $Ce/Ce^* = (Ce)_N/(2 \times (Pr)_N\text{-}(Nd)_N)$, where $(REE)_N$ refers to the concentrations normalized to Post-Archean Australian Shale (PAAS) values (Taylor and McLennan, 1985). A Ce anomaly value of less than 1 is indicative of a negative anomaly. Conversely, reduction reactions in sediments or anoxic waters typically release redox-sensitive elements such as Ce, Fe, and Mn (Zheng et al., 2016). As shown in Fig. 5, the Ce anomaly at the traditional stations exhibits a strong negative anomaly, decreasing to below 0.1 at a depth of 300 m. In contrast, the negative Ce anomalies were weak at depths of ~300–1000 m at stations K13/13a and K12/12a, where they remain above 0.1. At station K13, the Ce anomaly reaches its peak in winter (0.23 ± 0.08) at depths of 300–1000 m, while in summer and spring, the anomalies are 0.13 ± 0.02 and 0.12 ± 0.02, respectively. By station K11/11a, the Ce anomaly values align closely with those observed at the traditional stations.

4. Discussion

4.1. Seasonal variations of REE scavenging above the DCM

The lowest concentrations of REEs above the DCM (<~150 m) were observed (Fig. 4g and h), where biological activity is pronounced. Additionally, Nd and Yb exhibited a significant negative correlation ($p < 0.05$) with chlorophyll-α concentrations at depths shallower than 200 m, in both summer and winter (Fig. 6). These findings indicate the substantial scavenging of dissolved REEs by biologically induced particles in the upper ocean. Notably, as detailed in Section 3.2, REE concentrations were higher in summer than in winter above the DCM (*t*-test, $p < 0.05$). Even in oligotrophic waters with very low biomass, significant seasonal variations in the impact of biological processes on REEs were observed. This point is supported by the observed chlorophyll-α concentrations, which were twice as high in winter compared to summer in the upper water column (<200 m). The annual variation in chlorophyll concentrations, with a peak in winter, has also been observed in the western Pacific using satellite-based datasets and optical sensors (Hou et al., 2016; Xing et al., 2021). Elevated chlorophyll-α levels during winter suggest enhanced biological activity, which likely results in a greater abundance of particles and, as a consequence, more pronounced scavenging and removal of dissolved REEs.

The lower REE concentrations observed in winter may also result from reduced inputs of dissolved REEs during this season. The transport of East Asian dust to the North Pacific predominantly occurs in late winter and spring (e.g., Kanatani et al., 2014; Lee et al., 2015). Data from the MRREA-2 (Modern-Era Retrospective analysis for Research and Applications, version 2; http://giovanni.gsfc.nasa.gov/giovanni/) further indicate that total dust deposition flux in the Northwest Pacific increases gradually during winter and reaches its lowest levels in July and August (Kim et al., 2023). This suggests that atmospheric deposition fluxes in the region are higher in winter than in summer. Additionally, the diapycnal diffusion coefficient at 200 m depth showed no significant seasonal variation in magnitude, with values of $(2.1 \pm 1.5) \times 10^{-6}$ m^2/s in summer and $(2.7 \pm 3.4) \times 10^{-6}$ m^2/s in winter (Chuanjun Du, unpublished results). There is no significant seasonal difference in REE concentrations below the DCM (*t*-test, $p > 0.05$). However, REE concentrations above the DCM were lower in winter than in summer, leading to a larger vertical REE concentration gradient (dC/dZ) in winter. Consequently, the vertical flux of REEs from deeper layers is greater in winter compared to summer. In summary, above the DCM, REE concentrations due to both atmospheric deposition and vertical transport are higher in winter than in summer. However, REE concentrations were observed to be lower in winter than in summer above the DCM. This indicates that scavenging processes, particularly biological scavenging, are more intense in winter than in summer, resulting in lower REE concentrations above the DCM layer during winter.

Despite the similarity in ionic radii between Y and Ho, Ho demonstrates a superior complexing ability with organic ligands on marine particles compared to Y (Zhang et al., 1994; Nozaki et al., 1997). Above the DCM in the study area, we observed a pronounced fraction between Y and Ho (as indicated by the Y/Ho atomic ratio), which was markedly higher than in deep waters (Fig. 7). This observation aligns with findings from other studies in the Pacific (Zhang et al., 1994; Nozaki et al., 1997), underscoring the significant role of scavenging in the cycling of REE in open ocean. Furthermore, the Y/Ho atomic ratios were higher in winter (ranging from 115 to 184) compared to summer (ranging from 103 to 157) (t-test, $p < 0.05$), supporting the suggestion that scavenging is more intense in winter. Although LREEs are generally preferentially scavenged over HREEs, the Yb/Nd ratios did not exhibit statistically significant variation between summer and winter (t-test, $p > 0.05$). This

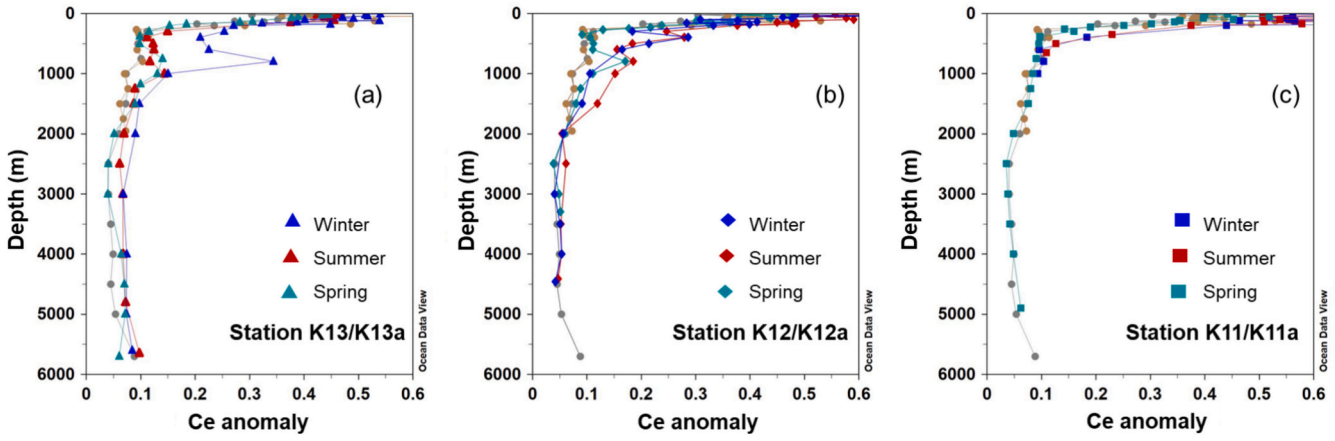

Fig. 5. Vertical profiles of Ce anomalies at stations K11/11a (square), K12/12a (diamond), and K13/13a (triangle) during (blue), summer (red), and spring (green). Dots represent measurements from other stations not affected by margin, as indicated by stations K9 and K10 reported by Cao et al. (2024). (For interpretation of the references to colour in this figure legend, the reader is referred to the web version of this article.)

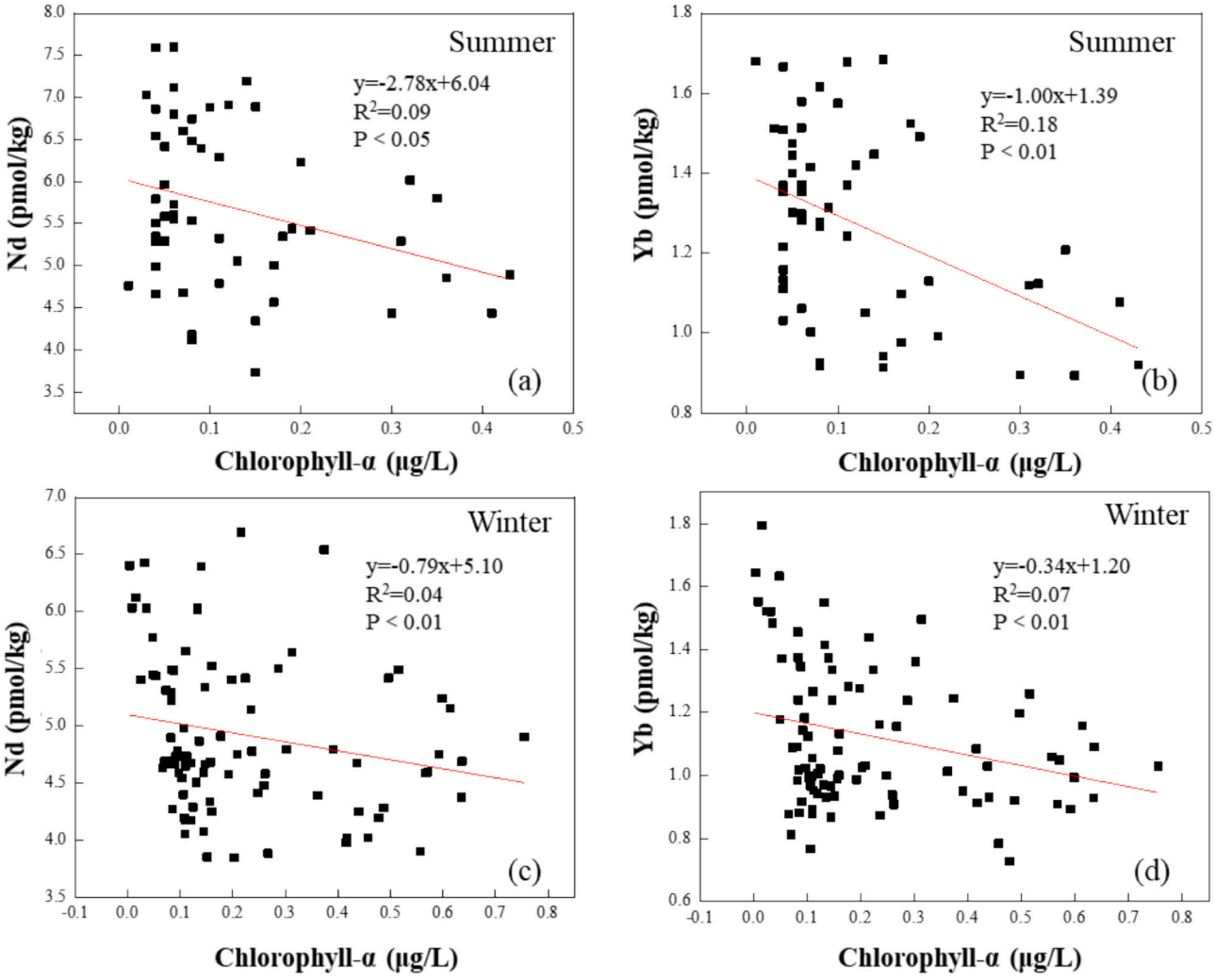

Fig. 6. Relationships between Nd (pmol/kg) and chlorophyll-α (μg/L) (a, c), and Yb (pmol/kg) and chlorophyll-α (μg/L) (b, d) during summer (a, b) and winter (c, d) for seawater at depths less than 200 m. The data for chlorophyll-α were sourced from Zhang et al. (2025, in press).

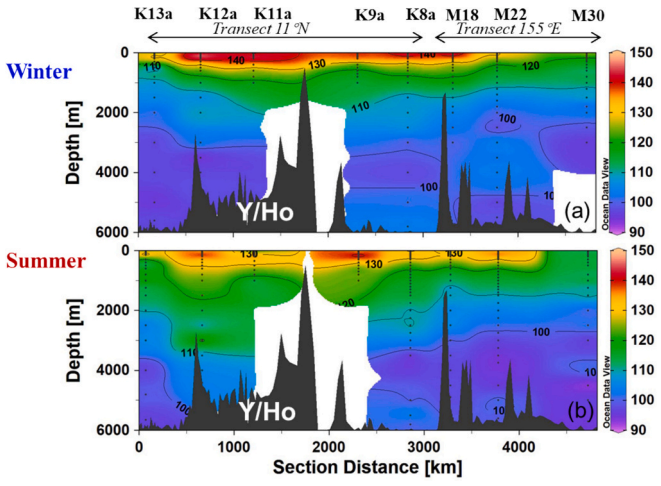

Fig. 7. Distributions of the Y/Ho ratios along the transects 11°N and 155°E in both winter (a) and summer (b).

indicates that the Y/Ho ratio is more sensitive to scavenging processes and is a more effective tool for tracking these processes.

To better understand the behavior of individual REEs during the scavenging process, we calculated the percentage reduction in concentration between the two cruises, using the initial summer concentration as a baseline. Since scavenging is the primary driver of REE reduction, this percentage was approximated as the scavenging efficiency. It should

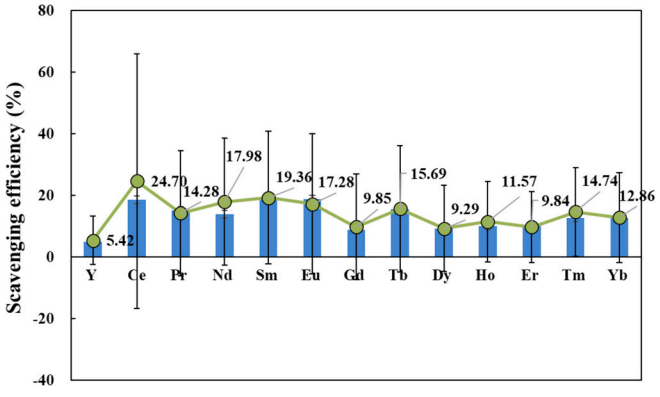

Fig. 8. Percentage reduction (referred to as scavenging efficiency (%)) in concentration for individual REEs. The bar graphs display the means and standard errors, with green dots and numbers indicating the medians. (For interpretation of the references to colour in this figure legend, the reader is referred to the web version of this article.)

be noted that this scavenging efficiency result is likely underestimated due to the oversight of substantial inputs in winter. The results, illustrated in Fig. 8, indicate that the scavenging efficiency of Y was lower compared to the other examined REEs. No significant difference ($p > 0.05$, $n = 52$) was observed in the scavenging efficiency of Yb and Nd. In contrast, a significant difference ($p < 0.05$, $n = 52$) was found between Y and Ho, which may suggest distinct removal mechanisms for these elements. Indeed, the observed deviation of Y from Ho and other REEs is likely attributed to the competitive interactions of particulate matter. Firstly, high Y/Ho ratios reflect differences in the complexation behavior of Y and Ho with inorganic ligands in seawater and soft organic ligands on the surfaces of particulate matter. This results in Y^{3+} being less reactive with particles compared to Ho^{3+} in seawater (Bau, 1996; Nozaki et al., 1997). Additionally, compared to Y, Ho exhibits more covalent bonding due to the involvement of 4f orbitals (Mioduski, 1993). During the incorporation of $REE(CO_3)^{2-}$ complexes (the predominant species in seawater) into calcite, Ho is incorporated more rapidly than Y, with Ho being removed nearly twice as fast as Y (Qu et al., 2009; Tanaka et al., 2008; Zhao et al., 2022). This observation is consistent with our findings, where the scavenging efficiency of Ho (averaging 10 ± 13 %) is approximately twice that of Y (averaging 5 ± 8 %) (Fig. 8).

4.2. Spatial variability and seasonal stability in REE release efficiency during remineralization

In the open ocean, remineralization plays a crucial role in shaping the vertical distribution of REEs in seawater. During remineralization, REEs adsorbed onto particles in the upper layer are released back into seawater as these particles sink (Stichel et al., 2015; Lambelet et al., 2016). AOU reflects the oxygen consumed during remineralization within a water parcel after its last contact with the atmosphere (Fitzsimmons et al., 2015). Below the DCM (~150 m–1000 m), we conducted linear regressions between REE concentrations (specifically Nd) and AOU, excluding stations K13/13a and K12/12a where external inputs in the intermediate water were identified (see Section 4.3.1 for details). The slopes of the linear fits between Nd and AOU were 0.05 ± 0.002 ($n = 145$, $R^2 = 0.82$, $p < 0.01$) in summer and 0.04 ± 0.003 ($n = 54$, $R^2 = 0.76$, $p < 0.01$) in winter, generally consistent with those reported for autumn (0.04 ± 0.003) and spring (0.04 ± 0.002) in NPSG (Behrens et al., 2018; Cao et al., 2023, 2024). This consistency suggests that variations in upper water column biomass do not significantly influence the efficiency of REE release during remineralization in the NPSG.

Spatial variations in the efficiency of REE release during remineralization are evident across different oceanic basins. For example, in the North Atlantic Gyre (15°–40°N; 200–1000 m), the slope of the linear relationship between Nd and AOU (0.04 ± 0.002; Stichel et al., 2015) is comparable to that observed in the NPSG at similar latitudes in this study (11°-33°N). This similarity suggests that the mechanisms governing REE release during remineralization in these subtropical gyres are similar. Both regions are dominated by *Prochlorococcus* within their microzooplankton communities (Campbell and Vaulot, 1993; Zubkov et al., 2000; Zhang et al., 2008), and the consistency in zooplankton community structure likely contributes to the observed similarities in REE release efficiency. While in the high-latitude mixing region of the Kuroshio Extension and Oyashio (35°–40°N), the slope of Nd versus AOU is significantly higher at 0.15 ± 0.005 (Cao et al., 2023), approximately four times greater than in the NPSG and North Atlantic Gyre. This region differs in plankton community structure, with *prochlorococcus* nearly absent and the community dominated by *picoeukaryotes* and heterotrophic bacteria (Zhang et al., 2008). These observations indicate that the efficiency of REE release during remineralization in the open ocean varies considerably, likely driven by differences in plankton community structure (Yamaguchi et al., 2004; Zhang et al., 2008; Zang et al., 2023).

The consistent ratio between Nd and AOU from subsurface to intermediate depths at specific latitudes provides valuable insights into REE cycling and allows for the prediction of Nd distribution. For example, in regions such as the NPSG and the North Atlantic Gyre, the Nd/AOU ratios were consistently around 0.04. Deviations from this established ratio may indicate the presence of sources or sinks of REEs that are not related to oxygen consumption. Conversely, the distribution of REEs from subsurface to intermediate depths (approximately 150–1000 m) can be effectively predicted using the Nd/AOU ratio in conjunction with observed AOU values, especially in regions remote from terrestrial sources. DO data, which can be obtained with high spatial resolution using DO sensors, provide a more readily available measure compared to REEs. Moreover, the Nd/AOU ratio has important potential applications in marine science, particularly for distinguishing and understanding various marine environments and processes. Firstly, this ratio is influenced by plankton community structure, allowing it to be used to qualitatively differentiate plankton communities. Secondly, when combined with the Redfield ratio, the Nd/AOU ratio can help establish an empirical relationship between Nd and dissolved organic carbon during the remineralization of organic particulate matter. This relationship is particularly valuable for studying the carbon cycle. For instance, at sites devoid of significant sources or sinks of REEs and organic carbon, the rate of Nd remineralization can be determined by correlating its concentration with the oxygen utilization rate, which in turn allows for the conversion of Nd remineralization rates into rates of organic carbon remineralization.

4.3. External sources of REEs in intermediate and deep water

4.3.1. Seasonal variations in lateral transport of REEs from sediment sources at intermediate water

In a previous spring cruise, weak Ce-negative anomalies were observed in intermediate waters (~800 m) near the Philippine Islands (stations K12, K13, and K14), which were attributed to slope sediment inputs and water mass transport (Cao et al., 2024). Similarly, increases in negative Ce anomalies were noted at 500–1000 m at stations K13a/K13 and K12a/K12 during the summer and winter cruises of this study as stated in Section 3.2 (Fig. 5a and b). At station K11a/K11, located farther from the island, this signal diminished, likely due to dilution or scavenging effects (Fig. 5c). Additionally, as depicted in Fig. 9, the PAAS-normalized Yb to Nd ratios (Yb/Nd) in intermediate seawater at

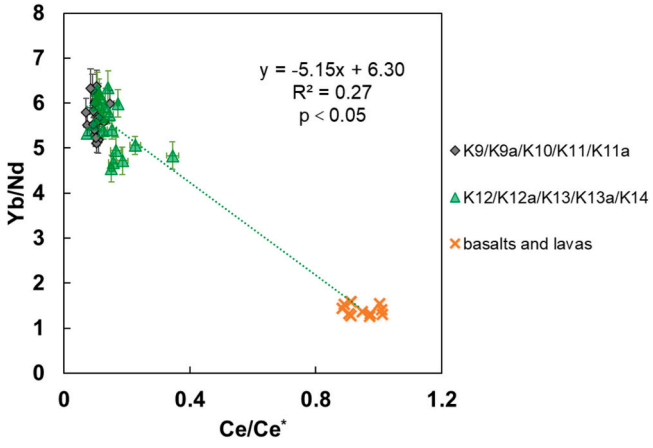

Fig. 9. The relationships show Yb/Nd ratios and Ce anomalies in intermediate waters (500–1000 m) at stations close to the islands (K12, K12a, K13, K13a, and K14), accompanied by linear fit curves. For comparison, data from stations farther from the islands (K9, K9a, K10, K11, and K11a) are also shown, along with reference values from basalts and lavas of the Philippine islands (Castillo and Newhall, 2004). Error bars reflect the analytical uncertainties associated with each element. The data of seawater from this study and Cao et al. (2024).

stations near the islands showed a slight decrease (below ~5). A strong correlation between the Yb/Nd ratios and the Ce/Ce* was observed, highlighting the influence of a specific source. Notably, the relationship between Yb/Nd ratios and Ce anomalies in basaltic and lava from the Philippine Islands (data from Castillo and Newhall, 2004) aligns with the extension of the linear fit line, further supporting that REE alterations in intermediate seawater at stations K12 to K14 originate from material inputs from the Philippine Islands.

Seasonal variations in the inputs from slope sediments on the Philippine Islands were evident in the modification of dissolved Nd and Ce anomalies. At a depth of 1000 m, the increase in Ce anomalies was most pronounced during the winter (Fig. 5), accompanied by elevated Nd concentrations (19.4 ± 0.9 pmol/kg in winter compared to 14.3 ± 0.4 pmol/kg and 13.1 ± 0.4 pmol/kg in summer and spring, respectively). As reported in previous studies, the persistent anticyclonic eddy located east of the Philippines plays a significant role in transporting lithogenic material from slope sediments into the open ocean (Cao et al., 2024). Moreover, seasonal variations in the strength of this eddy may influence the flux of material transport. Samplings at stations K13/K13a were conducted in June 2019 (spring, GP09), August 2020 (summer, GPpr15), and January 2021 (winter, GPpr15). In the region spanning 125°–130°E and 10°–14°N, mean eddy kinetic energy is highest from January to March (Zhang et al., 2021). This pattern aligns with our observations of the Ce anomaly signal at stations K13a/K13, suggesting that the seasonal variation in the modification of dissolved REEs by slope sediments may be primarily driven by the strength of the eddy.

Traditionally, below the DCM, REEs are thought to primarily originate from remineralization processes. However, input from external sources, such as slope sediments, was observed in the intermediate waters at stations K13/13a and K12/12a. To evaluate the contribution of this external source to the REE distributions, we divided transect 11°N into two sub-regions: stations with external inputs (stations K13/13a and K12/12a) and the margin-unaffected stations (stations K8-K11/11a). We established a relationship between Nd and AOU at stations K8-K11/11a, resulting in the fitting equation: $y = 0.037(\pm0.002)x + 3.04(\pm0.30)$ (Fig. 10). It was assumed that, in the absence of external inputs, the efficiency of Nd release through remineralization (0.037 ± 0.002) and the pre-formed Nd concentrations (3.04 ± 0.30) at stations K8-K11/11a would be constant. We estimated the theoretical Nd concentrations in the absence of external sources (referred to as predicted Nd concentrations) based on the observed AOU at stations K12/12a and K13/13a and the fitting equation of Nd to AOU. The Nd concentrations attributable to external sources were then determined by the difference between observed and predicted values (as shown in Table 1). The results indicated that at stations K12/12a and K13/13a, within the 500–1000 m depth range, external sources significantly contributed to

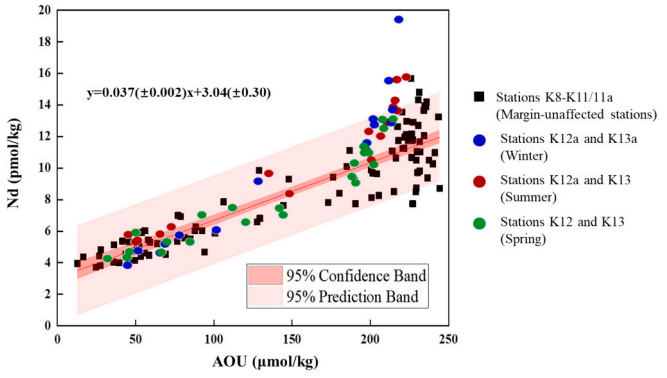

Fig. 10. Nd concentration (pmol/kg) versus AOU (μmol/kg) for stations sampled at depths of 150–1000 m during summer and winter in this study, as well as during spring in Cao et al. (2024). The fitting formula is derived from data at margin-unaffected stations (K8 to K11/11a). Colored dots represent stations K12/12a and K13/13a across different seasons.

Table 1
Estimated additional Nd concentrations (pmol/kg) and their ratios to the observed concentrations (%) from 500 m to 1000 m at stations K13/13a and K12/12a.

		KK2007	KK2003	GP09
Additional Nd concentration (pmol/kg)	Average	4.0 ± 2.6	2.7 ± 1.5	1.4 ± 0.7
	Range	2.0–8.3	0.1–4.5	0.6–2.4
Ratio of additional Nd (%)	average	26 ± 11	18 ± 9	11 ± 5
	Range	15–43	1–29	5–18
Sampling date		January 2021	August 2020	June 2019
Season		winter	summer	spring

Nd concentrations during winter, accounting for 26 % ± 11 % (ranging from 15 % to 43 %) of the observed Nd concentrations (Table 1). This suggests that slope sediment may be a crucial contributor of REEs to intermediate waters with seasonal variations driven by changes in eddy kinetic energy.

4.3.2. *Assessment of REE source contributions: Settled particles vs extra sources*

During the summer and winter cruises in our study, as well as the spring cruise reported by Cao et al. (2024), elevated REE concentrations were observed in the deep water (>4500 m) at station K2/K3/K13/13a, and K14, located in the Philippine Basin. These concentrations were slightly higher compared to other stations in the deep waters (Fig. 4 in this study and Fig. 5 in Cao et al. (2024)). For example, Nd concentrations were approximately 4.5 pmol/kg higher (excluding the most northerly stations M35 and M30, which were not discussed here). Notably, at station K13, beam transmission gradually decreased from 3000 m, reaching a minimum in the bottom water (~5700 m) with a total reduction of 0.1–0.2 % (Supplementary Fig. S1), indicating the possible presence of resuspended particles. In contrast, no decrease in transmission was observed in the deep waters at the other stations. Although the decline in beam transmission was slight, it suggests the presence of additional particle sources beyond settled particles, which may contribute to the observed increase in REE concentrations. Considering that the thickest benthic nepheloid layers typically observed are only 1000–1500 m (Gardner et al., 2018), it is plausible that the 3000–5700 m layer contains elevated REEs not only from resuspended particulate matter from the seafloor but also might from terrestrial sources, likely originating from the Philippine Islands, as stations K2/K3/K13/13a, and K14 are located just east of the islands. In the Philippine Basin, cyclonic and anticyclonic circulations are present between 3000 and bottom (Zhai and Gu, 2020). These persistent circulations provide the hydrodynamic conditions necessary for the transport of lithogenic materials across the basin. In addition, elevated lead (Pb) levels were observed in the deep waters at stations K2, K3, K13, and K14 compared to other stations (K12 to K8) located far from Philippines islands during the GP09 cruise, with concentrations of 20 % to 200 % higher than at other stations below 3500 m. Notably, Pb concentrations from 1000 to 5000 m at station K14, located northwest of station K13 and closer to the ocean margin, were approximately twice as high as those in the deep waters of stations K12 to K8 (Kuanbo Zhou, personal communication). Recent studies have highlighted boundary exchange between sediment and seawater as a potentially significant process in marine Pb cycling (Chen et al., 2023 and references therein). The observed high Pb levels in the deep waters at stations K2, K3, K13, and K14 support the hypothesis of a material source from the lateral transport associated with the Philippine Islands. Notably, the REE compositions (e.g., Ce anomaly, Yb/Nd ratio, and MREE anomaly) of deep water at stations within the basin appear unchanged (Supplementary Fig. S2), likely due to the relatively minor contribution of additional input, estimated at only 17 ± 6 %, as calculated below.

According to Cao et al. (2024), the distribution of REEs in deep water in this area was primarily governed by water mass mixing, a

conservative process. Secondary influences include non-conservative processes such as the remineralization of organic matter, and the dissolution of siliceous particles, which release dissolved REEs and silicate (Cao et al., 2024). For LREE, the concentration of Nd beyond the contributions of water mass mixing does not show a significant correlation with AOU or dissolved silicate, indicating the presence of scavenging processes as well (Behrens et al., 2018; Cao et al., 2024). To quantify the contribution of the extra source to dissolved REEs near the Philippines island, we employed a three-end-member mixing model to analyze the mixing ratios of the deep water masses (>2000 m). Following this, the non-conservative behavior of REE (ΔREE) was estimated using the difference between the measured and predicted conservative values. The model and estimation methodology are described in detail by Cao et al. (2024). Due to the stability of deep water mass properties and the lack of seasonal variability in REE concentrations, we conducted a comprehensive analysis of the ΔREE data from the three cruises. The result showed that the non-conservative components of Nd (ΔNd/Nd ratios) in deep water (≥4500 m) near the Philippines islands were higher than those in other stations (Fig. 11), further supporting the presence of additional inputs. The ΔNd significantly positively correlated with AOU ($n = 120$, $R^2 = 0.62$, $p < 0.01$), and with silicate (n = 120, $R^2 = 0.57$, $p < 0.01$) (Supplementary Fig. S3), suggesting that ΔNd is influenced by the remineralization of organic particles and the dissolution of siliceous particles (excluding stations K2/K2b, K3, K13/13a, and K14). This finding differs slightly from those of Cao et al. (2024), likely due to the larger dataset used in our analysis, which yielded more reliable conclusions. Therefore, it is assumed that the ΔREE in the deep water (except stations K2/K2b, K3, K13/13a, and K14) represents the effect of settled particles.

The ΔNd discrepancy in the deep water (>4500 m) between stations within the Philippines Basin (stations K2/K2b, K3, K13/13a, and K14) and others was used to obtain the contributions of REEs from additional sources. Below 4500 m depth at stations in the Philippine Basin, it is assumed that the non-conservative behavior of REEs is attributable to the release from both settled particles and extra sources, with ΔNd estimated at 27 ± 3 %. For other stations (excluding station K8a, where potential scavenging or dilution effects may occur as reported by Cao et al. (2024)), the non-conservative behavior of REEs is solely attributed to settled particles, with ΔNd accounting for 10 ± 5 %. The difference between these two values represents the contribution of extra sources, estimated at 17 ± 6 % for Nd. Despite uncertainties in this estimate, it can be inferred that settled particles and extra sources contribute roughly equivalent proportions (10 ± 5 % vs. 17 ± 6 %) to the dissolved Nd at the deep waters in the Philippine Basin, while deep water masses contribute 73 ± 3 % of the dissolved Nd in these deep waters. In other stations, the contributions of Nd from settled particles and deep water masses were 10 ± 5 % and 90 ± 5 %, respectively. Given that the proportions of ΔYb in observed Yb concentration were less than 10 %, and considering potential estimation errors, the elevated Yb in the deep water in the study area is predominantly controlled by water mass (>90 %).

On continental shelves and slopes, excess particles may be widespread in seawater, like nepheloid layers, which are formed by high-speed deep-sea currents. These layers contain significantly higher concentrations of suspended particles compared to the surrounding seawater (Gardner et al., 2018; Tian et al., 2022). The abundance of particulate matter within these nepheloid layers enhances the exchange of REEs between seawater and particles, potentially playing an important role in boundary exchange processes. In the Northern Atlantic, elevated concentrations of dissolved and particulate REEs have been observed in conjunction with the presence of nepheloid layers (Stichel et al., 2015; Crocket et al., 2018; Lagarde et al., 2020). Conversely, other studies have reported decreases in dissolved REEs associated with these layers (Lambelet et al., 2016; Morrison et al., 2019; Huang et al., 2023). These findings suggest that excess particles in the ocean, such as those found in nepheloid layers characterized by high particle mass, act as significant sources or sinks of dissolved REEs. Their impact on REEs should be included in the estimation of the REE mass balance in the global ocean.

4.4. Yb as a tracer for LCDW

Yb is the most chemically stable of the HREEs we analyzed in seawater, with a residence time of 2440 years (Zhang et al., 2019), making it a potential water mass tracer in deep water. Although a good correlation between ΔYb and both AOU and Si was observed in deep waters deeper than 2000 m, as discussed in Section 4.3 and reported by Cao et al. (2024), ΔYb represents a very small fraction (<~10 %) at depths beyond 4000 m. Therefore, Yb is dominantly controlled by water mass mixing (~90 %-100 %) and is conservative in the deep water of NPSG.

NPDW is the oldest deep water in the Pacific, originating from upwelled bottom waters in the north (Talley et al., 2011). Characteristic values for NPDW include a potential temperature of 1.76 ± 0.03 °C, a salinity of 34.60 ± 0.01, and a Yb concentration of 10.6 ± 0.3 pmol/kg (data north of 40°N from Piepgra and Jacobsen (1992) and stations D6 and E4 from the Kuroshio Extension cruise, Supplementary Table S5). LCDW, formed in the Southern Ocean (Talley et al., 2011), crosses the

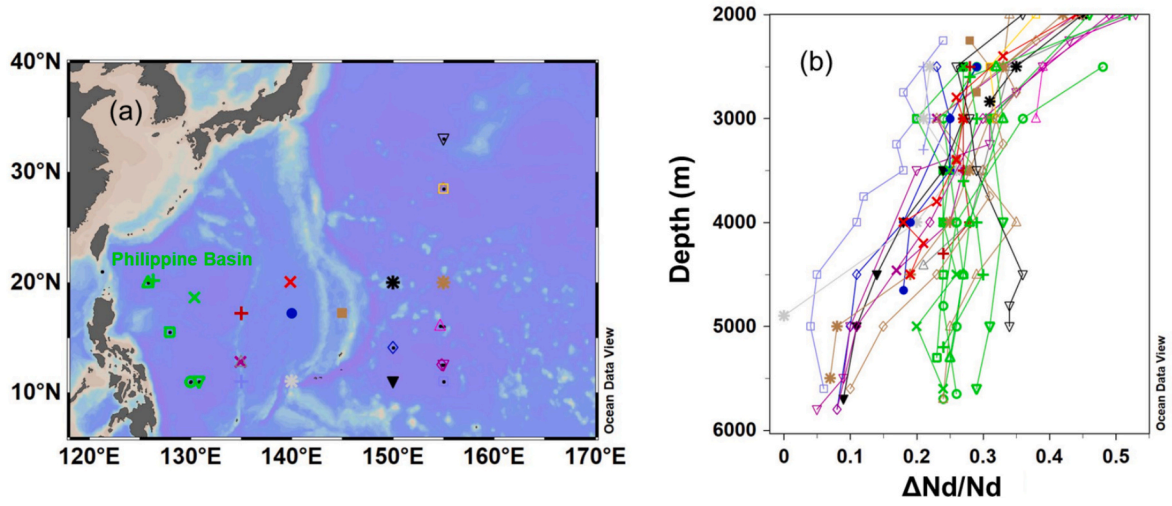

Fig. 11. Map showing ΔNd/Nd ratios in deep water in stations from this study and Cao et al. (2024). ΔNd represents the difference between observed Nd concentration and concentration calculated from water mass mixing. The positive ΔNd/Nd ratio indicates the addition of Nd relative to the observed concentration.

equator into the Northwest Pacific. It is characterized by relatively lower salinity (34.70 ± 0.02) and potential temperature (1.02 ± 0.73 °C), as well as relatively lower Yb concentration (7.3 ± 0.02 pmol/kg). These characteristics are based on data collected south of 20°S (Zhang and Nozaki, 1996; Molina-Kescher et al., 2014). In this study area, LCDW is characterized by a potential temperature below 1.2 °C (Johnson and Toole, 1993; Johnson et al., 1994; Tian et al., 2021; Wang et al., 2023). Below 4000 m, LCDW with low Yb concentrations is primarily mixed with NPDW that has high Yb concentrations (Behrens et al., 2018; Cao et al., 2024). Based on DO levels observed at depths below 4000 m, which range from 150 to 180 μmol/kg (Cao et al., 2024), it is evident that the high-oxygen Antarctic Bottom Water (AABW), with typical DO concentrations greater than 220 μmol/kg (Gunn et al., 2023), has not significantly penetrated the Philippine Sea. This further supports the dominance of LCDW at these depths. Additionally, significant correlations ($p < 0.01$) between Yb and potential temperature and salinity highlight the influence of water mass mixing on Yb distribution. These findings suggest that Yb has the potential as a tracer for the mixing of deep water masses.

At a depth of 4500 m, as illustrated in Fig. 12a, the Yb concentration was lowest in the Eastern Mariana Basin (EMB) at 9.3 ± 0.4 pmol/kg, increased to 9.9 ± 0.1 pmol/kg in the Western Mariana Basin (WMB), and reached 10.2 ± 0.1 pmol/kg in the Northern Philippine Basin (NPB), a value close to the Yb concentration characteristic of the NPDW end-member. This pattern indicates that LCDW with low Yb concentrations reaches the EMB and the WMB, with little to no penetration into the 4500 m in NPB. The near absence of a potential temperature below 1.2 °C at 4500 m in the NPB further supports this observation (Fig. 12b). While at 5500 m in the NPB, the Yb concentration is 9.9 pmol/kg, and the potential temperature decreases to nearly 1.2 °C. This observation indicates LCDW may reach the 5500 m depth in the NPB. This finding is consistent with previous reports indicating that LCDW enters the WMB from the EMB via the Yap Mariana Junction, and subsequently moves into the NPB through the Kyushu-Palau Ridge. The upper boundary of this water mass descends from approximately 4000 m in the WMB to ~5000 m in the NPB (Tian et al., 2021). This supports the reliability of Yb as a tracer for the LCDW water mass pathway in the study area.

5. Conclusions

We conducted seasonal sampling of REEs in the NPSG based on two GEOTRACES-CHINA process study cruises (GPpr15) to elucidate seasonal variations in REE cycling and the role of biological processes. Above the DCM, REE concentrations were significantly lower in winter compared to summer, reflecting enhanced scavenging by particulate matter driven by seasonally varying biological processes. No significant seasonal variations were observed in the release efficiency of REEs during remineralization (Nd to AOU ratio) across subsurface to intermediate depths (from 150 m to 1000 m) throughout the year. Spatially, the release efficiencies in this study area (NPSG) and the North Atlantic Gyre were comparable (~0.04 pmol Nd/μmol apparent oxygen utilization), attributable to the similar plankton community structures in both gyres. This consistent ratio holds potential for applications in tracing external sources, characterizing plankton community structures, and estimating remineralization rates of organic carbon.

Seasonal variations in Ce anomaly signals were associated with corresponding changes in eddy kinetic energy, indicating the lateral transport of sediments by water masses in mid-water depths near the Philippine Islands (500–1000 m at stations K12 and K13). The contribution of Nd from lateral transport is most significant during winter, accounting for 26 % ± 11 % (ranging from 15 % to 43 %) of the observed Nd, with contributions of 18 % ± 9 % (ranging from 1 % to 29 %) in summer and 11 % ± 5 % (ranging from 5 % to 18 %) in spring. In deep waters within the Philippine Basin, the elevated REE concentrations indicated a significant input of additional sources beyond settled particles. This extra input contributes to Nd concentrations at levels comparable to those from the remineralization or dissolution of settled particles (17 ± 6 % vs. 10 ± 5 %). At boundaries such as continental shelves and slopes, excess particles, including nepheloid layers, are widespread. These particles can act as either a source or a sink for seawater REEs and should be included in the global REE budget.

At a depth below 4000 m in the Northwest Pacific, Yb is predominantly influenced by water masses, accounting for over ~90 % of its variability. At a depth of 4500 m, changes in Yb concentration trace the distribution of LCDW as it reaches the EMB and the WMB before sinking in the NPB. With climate change and temperature change in deep water, relying solely on temperature and salinity to resolve water masses may introduce bias. Conservative chemical elements, such as Yb, offer valuable enhancements to traditional water mass tracers. This study reveals the seasonal-scale variations of REEs in seawater and identifies key controlling factors, thereby advancing our understanding of REE cycling. Furthermore, this study underscores the potential of REEs as tracers for tracking the LCDW pathway, particularly as valuable complementary tracers when deep water temperatures are disrupted.

Declaration of generative AI and AI-assisted technologies in the writing process

During the preparation of this work the author(s) used Doubao in order to improve the language. After using this tool/service, the author (s) reviewed and edited the content as needed and take(s) full responsibility for the content of the publication.

CRediT authorship contribution statement

Axiang Cao: Writing – original draft, Formal analysis, Data curation,

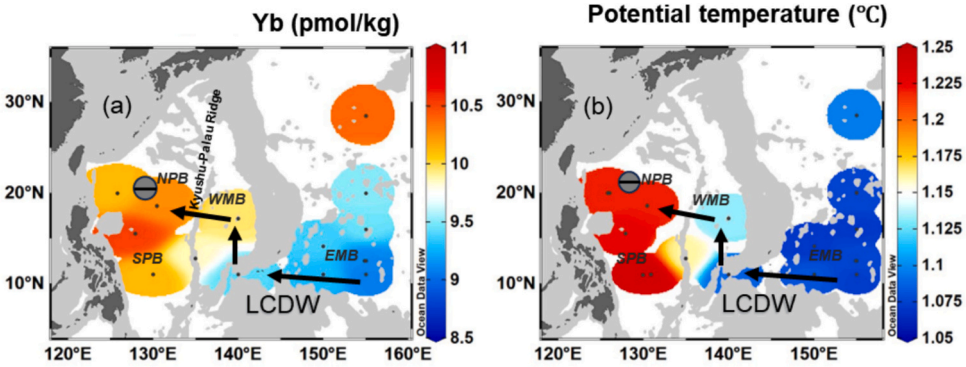

Fig. 12. Distributions of (a) Yb (pmol/kg) and (b) potential temperature (°C) at a depth of 4500 m in stations from this study and Cao et al. (2024). NPB: Northern Philippine Basin; SPB: Southern Philippine Basin; WMB: West Mariana Basin; EMB: East Mariana Basin. Arrows represent the pathway of LCDW, while circles indicate the deepening of potential temperature isotherms and the upper interface of LCDW.

Conceptualization. **Qian Liu:** Writing – review & editing, Supervision, Project administration, Conceptualization. **Jing Zhang:** Writing – review & editing, Supervision, Project administration, Conceptualization. **Zhensong Liu:** Data curation. **Jingling Ren:** Writing – review & editing. **Yihua Cai:** Writing – review & editing. **Kuanbo Zhou:** Writing – review & editing. **Xianghui Guo:** Writing – review & editing, Data curation. **Xin Liu:** Writing – review & editing, Data curation, Investigation, Methodology.

Declaration of competing interest

The authors declare that they have no known competing financial interests or personal relationships that could have appeared to influence the work reported in this paper.

Acknowledgments

We thank the captain and crew of the R/V TAN KAH KEE for their help with sampling. We are also thankful to Wenkai Guan, Jing Chen, and Wanyang He for their help in collecting samples. We would like to thank Prof. Bangqin Huang from Xiamen University for providing the chlorophyll-α data, and Dr. Chuanjun Du from Hainan University for supplying the diffusion coefficient data during the cruises. We also appreciate Prof. Lei Han from Xiamen University Malaysia for his valuable guidance, which helped improve the manuscript. We also thank Tiying Jiao for her help with the figures in this paper. This research was supported by the National Key Research and Developmental Program of China (Grant 2023YFF0805001), National Natural Science Foundation of China (Grant 41890801), and JSPS KAKENHI (Grants JP20H04319, JP22H05206).

Appendix A. Supplementary data

The supplemental file includes information related to the data of hydrographic parameters, REE concentrations, and vertical profiles of beam transmission in the study area, etc.

Data availability

Data will be made available on request.

References

Abbott, A.N., Haley, B.A., McManus, J., 2015a. Bottoms up: Sedimentary control of the deep North Pacific Ocean's εNd signature. Geology 43, 1035–1038. https://doi.org/10.1130/G37114.1.

Abbott, A.N., Haley, B.A., McManus, J., Clare, E.R., 2015b. The sedimentary flux of dissolved rare earth elements to the ocean. Geochim. Cosmochim. Acta 154, 186–200. https://doi.org/10.1016/j.gca.2015.01.010.

Alibo, D.S., Nozaki, Y., 1999. Rare earth elements in seawater: particle association, shale-normalization, and Ce oxidation. Geochim. Cosmochim. Acta 63, 363–372. https://doi.org/10.1016/S0016-7037(98)00279-8.

Bau, M., 1996. Controls on the fractionation of isovalent trace elements in magmatic and aqueous systems: evidence from Y/Ho, Zr/Hf, and lanthanide tetrad effect. Contrib. Mineral. Petrol. 123, 323–333. https://doi.org/10.1007/s004100050159.

Behrens, M.K., Pahnke, K., Paffrath, R., Schnetger, B., Brumsack, H.J., 2018. Rare earth element distributions in the West Pacific: trace element sources and conservative vs. non-conservative behavior. Earth Planet. Sci. Lett. 486, 166–177. https://doi.org/10.1016/j.epsl.2018.01.016.

Bertram, C.J., Elderfield, H., 1993. The geochemical balance of the rare earth elements and neodymium isotopes in the oceans. Geochim. Cosmochim. Acta 57, 1957–1986. https://doi.org/10.1016/0016-7037(93)90087-D.

Bostock, H.C., Sutton, P.J., Williams, M.J.M., Opdyke, B.N., 2013. Reviewing the circulation and mixing of antarctic intermediate water in the South Pacific using evidence from geochemical tracers and Argo float trajectories. Deep Sea Res. Part I Oceanogr. Res. 73, 84–98. https://doi.org/10.1016/j.dsr.2012.11.007.

Campbell, L., Vaulot, D., 1993. Photosynthetic picoplankton community structure in the subtropical North Pacific Ocean near Hawaii (Station ALOHA). Deep Sea Res. Part I Oceanogr. Res. Pap. 40, 2043–2060. https://doi.org/10.1016/0967-0637(93)90044-4.

Cantrell, K.J., Byrne, R.H., 1987. Rare earth element complexation by carbonate and oxalate ions. Geochim. Cosmochim. Acta 51, 597–605. https://doi.org/10.1016/0016-7037(87)90072-X.

Cao, A., Zhang, J., Zhang, H., Chen, Z., Cui, G., Liu, Z., Li, Y., Liu, Q., 2023. Dissolved rare earth elements in the Northwest Pacific: sources, water mass tracing, and cross-shelf fluxes. Front. Mar. Sci. 10, 1135113. https://doi.org/10.3389/fmars.2023.1135113.

Cao, A., Liu, Q., Zhang, J., Shiller, A.M., Cai, Y., Zhang, R., Gilbert, M., Guo, X., Liu, Z., 2024. Dissolved rare earth elements in the North Pacific Subtropical Gyre: lithogenic sources and water mass mixing control. Geochim. Cosmochim. Acta 372, 42–61. https://doi.org/10.1016/j.gca.2024.02.018.

Castillo, P.R., Newhall, C.G., 2004. Geochemical constraints on possible subduction components in lavas of Mayon and Taal Volcanoes, Southern Luzon, Philippines. J. Petrol. 45, 1089–1108. https://doi.org/10.1093/petrology/egh005.

Chen, M., Boyle, E.A., Jiang, S., Liu, Q., Zhang, J., Wang, X., Zhou, K., 2023. Dissolved lead (Pb) concentrations and Pb isotope ratios along the East China Sea and Kuroshio transect: evidence for isopycnal transport and particle exchange. J. Geophys. Res.: Oceans 128. https://doi.org/10.1029/2022JC019423 e2022JC019423.

Crocket, K.C., Hathorne, E.C., Abell, R.E., Baker, A.R., Jickells, T.D., Achterberg, E.P., 2018. Rare earth element distribution in the NE Atlantic: evidence for benthic sources, longevity of the seawater signal, and biogeochemical cycling. Front. Mar. Sci. 5, 147. https://doi.org/10.3389/fmars.2018.00147.

Dai, M., Luo, Y., Achterberg, E.P., Browning, T.J., Cai, Y., Cao, Z., Chai, F., Chen, B., Church, M.J., Ci, D., Du, C., Gao, K., Guo, X., Hu, Z., Kao, S., Laws, E.A., Lee, Z., Lin, H., Liu, Q., Liu, X., Luo, W., Meng, F., Shang, S., Shi, D., Saito, H., Song, L., Wan, X.S., Wang, Y., Wang, W., Wen, Z., Xiu, P., Zhang, J., Zhang, R., Zhou, K., 2023. Upper ocean biogeochemistry of the oligotrophic North Pacific Subtropical Gyre: from nutrient sources to carbon export. Rev. Geophys. 61. https://doi.org/10.1029/2022RG000800 e2022RG000800.

de Baar, H.J.W., German, C.R., Elderfield, H., van Gaans, P., 1988. Rare earth element distributions in anoxic waters of the Cariaco Trench. Geochim. Cosmochim. Acta 52, 1203–1219. https://doi.org/10.1016/0016-7037(88)90243-8.

de Baar, H.J.W., Bruland, K.W., Schijf, J., van Heuven, S.M.A.C., Behrens, M.K., 2018. Low cerium among the dissolved rare earth elements in the central North Pacific Ocean. Geochim. Cosmochim. Acta 236, 5–40. https://doi.org/10.1016/j.gca.2018.03.003.

Ebeling, A., Zimmermann, T., Klein, O., Irrgeher, J., Pröfrock, D., 2022. Analysis of seventeen certified water reference materials for trace and technology-critical elements. Geostand. Geoanal. Res. 46, 351–378. https://doi.org/10.1111/ggr.12422.

Elderfield, H., Greaves, M.J., 1982. The rare earth elements in seawater. Nature 296, 214–219. https://doi.org/10.1038/296214a0.

Fitzsimmons, J.N., Carrasco, G.G., Wu, J.F., Saeed, R., Horner, T.J., Measures, C.I., Conway, T.M., John, S.G., Boyle, E.A., 2015. Partitioning of dissolved iron and iron isotopes into soluble and colloidal phases along the GA03 GEOTRACES North Atlantic transect. Deep Sea Res. Part II: Top. Stud. Oceanogr. 116, 130–151. https://doi.org/10.1016/j.dsr2.2014.11.014.

Fröllje, H., Suzuki, K., Matsumoto, K., Wakita, M., Mino, Y., 2016. Seasonal variability of phytoplankton community structure in the subtropical western North Pacific. J. Oceanogr. 72, 343–358. https://doi.org/10.1007/s10872-015-0346-9.

Garcia-Solsona, E., Pena, L.D., Paredes, E., Pérez-Asensio, J.N., Quirós-Collazos, L., Lirer, F., Cacho, I., 2020. Rare earth elements and Nd isotopes as tracers of modern ocean circulation in the Central Mediterranean Sea. Prog. Oceanogr. 185, 102340. https://doi.org/10.1016/j.pocean.2020.102340.

Gardner, W.D., Richardson, M.J., Mishonov, A.V., 2018. Global assessment of benthic nepheloid layers and linkage with upper ocean dynamics. Earth Planet. Sci. Lett. 482, 126–134. https://doi.org/10.1016/j.epsl.2017.11.008.

Gebbie, G., Huybers, P., 2019. The little ice age and 20th-century deep Pacific cooling. Science 363, 70–74. https://doi.org/10.1126/science.aar8413.

Goldberg, E.D., Koide, M., Schmitt, R.A., Smith, R.H., 1963. Rare-earth distributions in the marine environment. J. Geophys. Res. 68, 4209–4217. https://doi.org/10.1029/JZ068i014p04209.

Gunn, K.L., Rintoul, S.R., England, M.H., Bowen, M.M., 2023. Recent reduced abyssal overturning and ventilation in the Australian Antarctic Basin. Nat. Clim. Chang. 13, 537–544. https://doi.org/10.1038/s41558-023-01667-8.

Haley, B.A., Du, J., Abbott, A.N., McManus, J., 2017. The impact of benthic processes on rare earth element and neodymium isotope distributions in the oceans. Front. Mar. Sci. 4, 426. https://doi.org/10.3389/fmars.2017.00426.

Hou, X., Dong, Q., Xue, C., Wu, S., 2016. Seasonal and interannual variability of chlorophyll-a and associated physical synchronous variability in the western tropical Pacific. J. Mar. Syst. 158, 59–71. https://doi.org/10.1016/j.jmarsys.2016.01.008.

Huang, Y., Christophe, C., Liu, Z.F., Eric, D., Arnaud, D., Frederic, H., Wu, Q., Andrew Lin, T.S., 2023. Impacts of nepheloid layers and mineralogical compositions of oceanic margin sediments on REE concentrations and Nd isotopic compositions of seawater. Geochim. Cosmochim. Acta 359, 57–70. https://doi.org/10.1016/j.gca.2023.08.026.

Johannesson, K.H., Burdige, D.J., 2007. Balancing the global oceanic neodymium budget: evaluating the role of groundwater. Earth Planet. Sci. Lett. 253, 129–142. https://doi.org/10.1016/j.epsl.2006.10.021.

Johnson, G.C., Toole, J.M., 1993. Flow of deep and bottom waters in the Pacific at 10°N. Deep-Sea Res. 40, 371–394. https://doi.org/10.1016/0967-0637(93)90009-R.

Johnson, G.C., Rudnick, D.L., Taft, B.A., 1994. Bottom water variability in the Samoa passage. J. Mar. Res. 52 (2), 177–196. https://doi.org/10.1357/0022240943077118.

Johnson, G.C., Mecking, S., Sloyan, B.M., Wijffels, S.E., 2007. Recent bottom water warming in the Pacific Ocean. J. Clim. 20, 5371–5375. https://doi.org/10.1175/2007JCLI1879.1.

Kanatani, K.T., Okumura, M., Tohno, S., Adachi, Y., Sato, K., Nakayama, T., 2014. Indoor particle counts during Asian dust events under everyday conditions at an apartment

in Japan. Environ. Health Prev. Med. 19 (1), 81–88. https://doi.org/10.1007/s12199-013-0356-4.
Karl, D.M., 1999. A sea of change: biogeochemical variability in the North Pacific Subtropical Gyre. Ecosystems 2, 181–214. https://doi.org/10.1007/s100219900068.
Kawabe, M., Fujio, S., 2010. Pacific Ocean circulation based on observation. J. Oceanogr. 66, 389–403. https://doi.org/10.1007/s10872-010-0034-8.
Kawabe, M., Fujio, S., Yanagimoto, D., 2003. Deep-water circulation at low latitudes in the western North Pacific. Deep Sea Res. Part I Oceanogr. Res. Pap. 50, 631–656. https://doi.org/10.1016/S0967-0637(03)00040-2.
Kawabe, M., Fujio, S., Yanagimoto, D., Tanaka, K., 2009. Water masses and currents of deep circulation southwest of the Shatsky Rise in the western North Pacific. Deep Sea Res. I 56, 1675–1687. https://doi.org/10.1016/j.dsr.2009.06.004.
Kim, H.J., Kim, D., Park, Y.-G., Park, J.-Y., Choi, K.-Y., Park, J.S., An, S.M., Kwon, K., Noh, J.H., Hwang, J., 2023. Influence of atmospheric dust deposition on sinking particle flux in the Northwest Pacific. Front. Mar. Sci. 10, 1180480. https://doi.org/10.3389/fmars.2023.1180480.
Kraemer, D., Schmidt, K., Klimpel, F., Rauch, U., Ernst, D.M., Paul, S.A.L., Haeckel, M., Koschinsky, A., Bau, M., 2024. Tracking the distribution of persistent and mobile wastewater-derived substances in the southern and Central North Sea using anthropogenic gadolinium from MRI contrast agents as a far-field tracer. Mar. Pollut. Bull. 207, 116794. https://doi.org/10.1016/j.marpolbul.2024.116794.
Labasque, T., Chaumery, C., Aminot, A., Kergoat, G., 2004. Spectrophotometric Winkler determination of dissolved oxygen: re-examination of critical factors and reliability. Mar. Chem. 88 (1–2), 53–60. https://doi.org/10.1016/j.marchem.2004.02.002.
Lagarde, M., Lemaitre, N., Planquette, H., Grenier, M., Belhadj, M., Lherminier, P., Jeandel, C., 2020. Particulate rare earth element behavior in the North Atlantic (GEOVIDE cruise). Biogeosciences 17, 5539–5561. https://doi.org/10.5194/bg-17-5539-2020.
Lambelet, M., van de Flierdt, T., Crocket, K., Rehkämper, M., Kreissig, K., Coles, B., Rijkenberg, M.J.A., Gerringa, L.J.A., de Baar, H.J.W., Steinfeldt, R., 2016. Neodymium isotopic composition and concentration in the western North Atlantic Ocean: results from the GEOTRACES GA02 section. Geochim. Cosmochim. Acta 177, 1–29. https://doi.org/10.1016/j.gca.2015.12.019.
Lee, Y.G., Ho, C.-H., Kim, J.-H., Kim, J., 2015. Quiescence of Asian dust events in South Korea and Japan during 2012 spring: dust outbreaks and transports. Atmos. Environ. 114, 92–101. https://doi.org/10.1016/j.atmosenv.2015.05.035.
Liao, X., Zhang, W., Yang, T., Hu, Z., Luo, T., Zeng, X., Zhou, L., 2023. Accurate determination of rare earth elements in small volumes of porewater from marine sediments by laser ablation solution sampling ICP-MS. J. Anal. At. Spectrom. 38 (1), 156–165. https://doi.org/10.1039/D2JA00236A.
Liu, Q., Zhang, J., He, H., Ma, L., Li, H., Zhu, S., Matsuno, T., 2022. Significance of nutrients in oxygen-depleted bottom waters via various origins on the mid-outer shelf of the East China sea during summer. Sci. Total Environ. 826, 154083. https://doi.org/10.1016/j.scitotenv.2022.154083.
Mioduski, T., 1993. Covalency of Sc(III), Y(III), Ln(III), and An(III) as manifested in the enthalpies of solution of anhydrous rare earth halides. J. Radioanal. Nucl. Chem. 176, 371–382. https://doi.org/10.1007/BF02034759.
Molina-Kescher, M., Frank, M., Hathorne, E., 2014. South Pacific dissolved Nd isotope compositions and rare earth element distributions: water mass mixing versus biogeochemical cycling. Geochim. Cosmochim. Acta 127, 171–189. https://doi.org/10.1016/j.gca.2013.11.038.
Morrison, R., Waldner, A., Hathorne, E.C., Rahlf, P., Zieringer, M., Montagna, P., Colin, C., Frank, N., Frank, M., 2019. Limited influence of basalt weathering inputs on the seawater neodymium isotope composition of the Northern Iceland Basin. Chem. Geol. 511, 358–370. https://doi.org/10.1016/j.chemgeo.2018.10.019.
Nozaki, Y., Zhang, J., Amakawa, H., 1997. The fractionation between Y and Ho in the marine environment. Earth Planet. Sci. Lett. 148, 329–340. https://doi.org/10.1016/S0012-821X(97)00034-4.
Oka, E., Qiu, B., 2012. Progress of North Pacific mode water research in the past decade. J. Oceanogr. 68, 5–20. https://doi.org/10.1007/s10872-011-0032-5.
Piepgra, D.J., Jacobsen, S.B., 1992. The behavior of rare earth elements in seawater: precise determination of variations in the North Pacific water column. Geochim. Cosmochim. Acta 56, 1851–1862. https://doi.org/10.1016/0016-7037(92)90315-A.
Qu, C.L., Liu, G., Zhao, Y.F., 2009. Experimental study on the fractionation of yttrium from holmium during the coprecipitation with calcium carbonate in seawater solutions. Geochem. J. 43, 403–414. https://doi.org/10.2343/geochemj.43.403.
Schijf, J., de Baar, H.J.W., Wijbrans, J.R., Landing, W.F., 1991. Dissolved rare earth elements in the Black Sea. Deep-Sea Res. 38, S805–S823. https://doi.org/10.1016/0198-0149(91)90033-8.
Schlitzer, R., 2016. Ocean Data View. http://odv.awi.de.
Schmidt, K., Paul, S.A.L., Achterberg, E.P., 2022. Assessing the availability of trace metals including rare earth elements in deep ocean waters of the Clarion Clipperton Zone, NE Pacific: application of an in situ DGT passive sampling method. Trends Anal. Chem. 155, 116657. https://doi.org/10.1016/j.trac.2022.116657.
Seo, H., Kim, G., 2020. Rare earth elements in the East Sea (Japan Sea): distributions, behaviors, and applications. Geochim. Cosmochim. Acta 286, 19–28. https://doi.org/10.1016/j.gca.2020.07.016.
Shannon, R.D., 1976. Revised effective ionic radii and systematic studies of interatomic distances in halides and chalcogenides. Acta Crystallogr. A 32, 751–767. https://doi.org/10.1107/S0567739476001551.
Siddall, M., Khatiwala, S., van de Flierdt, T., Jones, K., Goldstein, S.L., Hemming, S., Anderson, R.F., 2008. Towards explaining the Nd paradox using reversible scavenging in an ocean general circulation model. Earth Planet. Sci. Lett. 274, 448–461. https://doi.org/10.1016/j.epsl.2008.07.044.
Siedler, G.H.J., Müller, T.C., 2004. Deep-water flow in the Mariana and Caroline Basins. J. Phys. Oceanogr. 34, 566–581. https://doi.org/10.1175/2511.1.
Stichel, T., Alison, E., Hartman, B.D., Steven, L., Goldstein, H.S., Katharina, P., 2015. Separating biogeochemical cycling of neodymium from water mass mixing in the Eastern North Atlantic. Earth Planet. Sci. Lett. 412, 245–260. https://doi.org/10.1016/j.epsl.2014.12.008.
Suga, T., Kato, A.H., 2000. North Pacific tropical water: its climatology and temporal changes associated with the climate regime shift in the 1970s. Prog. Oceanogr. 47, 223–256. https://doi.org/10.1016/S0079-6611(00)00037-9.
Sun, C., Xu, J., Liu, Z., Tong, M., Zhu, B., 2008. Application of Argo data in the analysis of water masses in the Northwest Pacific Ocean. Mar. Sci. Bull. 25 (3), 1–13 (In Chinese).
Tachikawa, K., 2003. Neodymium budget in the modern ocean and paleo-oceanographic implications. J. Geophys. Res. 108, 3254. https://doi.org/10.1029/1999JC000285.
Takata, H., Tagami, K., Aono, T., Uchida, S., 2009. Determination of trace levels of yttrium and rare earth elements in estuarine and coastal waters by inductively coupled plasma mass spectrometry following preconcentration with NOBIASCHELATE resin. At. Spectrosc. 30, 10–19.
Talley, L.D., Pickard, G.L., Emery, W.J., 2011. Descriptive Physical Oceanography: An Introduction, 6th ed. Academic Press, Amsterdam; Boston.
Tanaka, K., Takahashi, Y., Shimizu, H., 2008. Local structure of Y and Ho in calcite and its relevance to Y fractionation from Ho in partitioning between calcite and aqueous solution. Chem. Geol. 248, 104–113. https://doi.org/10.1016/j.chemgeo.2007.11.003.
Taylor, S.R., McLennan, S.M., 1985. The Continental Crust, its Composition and Evolution: An Examination of the Geochemical Record Preserved in Sedimentary Rocks. Blackwell Scientific, Oxford.
Tazoe, H., Obata, H., Gamo, T., 2011. Coupled isotopic systematics of surface cerium and neodymium in the Pacific Ocean. Geochem. Geophys. Geosyst. 12, Q04004. https://doi.org/10.1029/2010GC003342.
Tian, Z., Zhou, C., Xiao, X., Wang, T.H., Qu, T.D., Yang, Q.X., Zhao, W., Tian, J.W., 2021. Water-mass properties and circulation in the deep and abyssal Philippine Sea. J. Geophys. Res. Oceans 126, 6. https://doi.org/10.1029/2020JC016994.
Tian, Z., Liu, Y., Zhang, X., Zhang, Y., Zhang, M., 2022. Formation mechanisms and characteristics of the marine nepheloid layer: a review. Water 2022 (14), 678. https://doi.org/10.3390/w14050678.
Tsuchiya, M., 1968. Upper waters of the intertropical Pacific Ocean. Johns Hopkins Oceanogr. Stud. 4, 50. https://doi.org/10.4319/lo.1969.14.4.0650c.
Wang, J.N., Wang, F., Lu, Y.Y., Zhang, H., Ma, Q., Pratt, L.J., Zhang, Z.X., 2023. Abyssal circulation from the Yap-Mariana junction to the Northern Philippine Basin. Geophys. Res. Lett. 50. https://doi.org/10.1029/2022GL100610 e2022GL100610.
Welschmeyer, N.A., 1994. Fluorometric analysis of chlorophyll a in the presence of chlorophyll b and pheopigments. Limnol. Oceanogr. 39, 1985–1992. https://doi.org/10.4319/lo.1994.39.8.1985.
Wunsch, C., Heimbach, P., 2014. Bidecadal thermal changes in the Abyssal Ocean. J. Phys. Oceanogr. 44, 2013–2030. https://doi.org/10.1175/JPO-D-13-096.1.
Xing, X., Boss, E., Chen, S., Chai, F., 2021. Seasonal and daily-scale photoacclimation modulating the phytoplankton chlorophyll-carbon coupling relationship in the mid-latitude Northwest Pacific. J. Geophys. Res. Oceans 126. https://doi.org/10.1029/2021JC017717 e2021JC017717.
Yamaguchi, A., Yuji, W., Hiroshi, I., Takashi, H., Kazushi, F., Shinya, S., Joji, I., Tsutomu, I., Masayuki, M.T., 2004. Latitudinal differences in the planktonic biomass and community structure down to the greater depths in the Western North Pacific. J. Oceanogr. 60, 773–787. https://doi.org/10.1007/s10872-004-5770-1.
Yu, Z., Colin, C., Meynadier, L., Douville, E., Dapoigny, A., Reverdin, G., Wu, Q., Wan, S., Song, L., Xu, Z., Bassinot, F., 2017a. Seasonal variations in dissolved neodymium isotope composition in the Bay of Bengal. Earth Planet. Sci. Lett. 479, 310–321. https://doi.org/10.1016/j.epsl.2017.09.022.
Yu, Z., Colin, C., Douville, E., Meynadier, L., Duchamp-Alphonse, S., Sepulcre, S., Wan, S., Song, L., Wu, Q., Xu, Z., Bassinot, F., 2017b. Yttrium and rare earth element partitioning in seawaters from the Bay of Bengal. Geochem. Geophys. Geosyst. 18, 1388–1403. https://doi.org/10.1002/2016GC006749.
Zang, Y., Chen, H., Zhuang, Y., Ge, R., Wang, W., Liu, G., 2023. Latitudinal transition of epipelagic mesozooplankton in the northwestern Pacific in winter. Mar. Environ. Res. 186, 105915. https://doi.org/10.1016/j.marenvres.2023.105915.
Zhai, F.G., Gu, Y.Z., 2020. Abyssal circulation in the Philippine Sea. J. Ocean Univ. China 19, 249–262. https://doi.org/10.1007/s11802-020-4241-7.
Zhang, J., Nozaki, Y., 1996. Rare earth elements and yttrium in seawater: ICP-MS determinations in the East Caroline, Coral Sea, and South Fiji basins of the western South Pacific Ocean. Geochim. Cosmochim. Acta 60, 4631–4644. https://doi.org/10.1016/S0016-7037(96)00276-1.
Zhang, J., Amakawa, H., Nozaki, Y., 1994. The comparative behaviors of yttrium and lanthanides in the seawater of the North Pacific. Geophys. Res. Lett. 21, 2677–2680. https://doi.org/10.1029/94GL02404.
Zhang, Y., Jiao, N.Z., Hong, N., 2008. Comparative study of picoplankton biomass and community structure in different provinces from subarctic to subtropical oceans. Deep Sea Res. Part II Top. Stud. Oceanogr. 55, 1605–1614. https://doi.org/10.1016/j.dsr2.2008.04.014.
Zhang, J., Liu, Q., Bai, L., Matsuno, T., 2018. Water mass analysis and contribution estimation using heavy rare earth elements: significance of Kuroshio intermediate water to Central East China Sea shelf water. Mar. Chem. 204, 172–180. https://doi.org/10.1016/j.marchem.2018.07.011.
Zhang, J., Liu, Q., He, Q., Nozaki, Y., 2019. Rare earth elements and their isotopes in the ocean. In: Cochran, J.K., Bokuniewicz, J.H., Yager, L.P. (Eds.), Encyclopedia of Ocean Sciences, 3rd Edition 1. Academic Press, pp. 181–197. https://doi.org/10.1016/B978-0-12-409548-9.10855-3.

Zhang, L.L., Hui, Y.C., Qu, T.D., Hu, D.X., 2021. Seasonal variability of subthermocline eddy kinetic energy east of the Philippines. J. Phys. Oceanogr. 51, 685–699. https://doi.org/10.1175/JPO-D-20-0101.1.

Zhang, Y., Huang, Y., Xu, F., Cai, S., Liu, Y., Xu, C., Lin, L., Chen, J., Laws, E.A., Liu, X., Huang, B., 2025. Decoupling of bacterial production and respiration in the surface water of the North Pacific Subtropical Gyre. Mar. Life sci. Technol. https://doi.org/10.1007/s42995-025-00279-9 in press.

Zhao, Y.Y., Wei, W., Santosh, Y., Hu, J., Wei, H.T., Yang, J., Liu, S., Zhang, G.L., Yang, D. D., Li, S.Z., 2022. A review of retrieving pristine rare earth element signatures from carbonates. Palaeogeogr. Palaeoclimatol. Palaeoecol. 586, 110765. https://doi.org/10.1016/j.palaeo.2021.110765.

Zheng, X.-Y., Plancherel, Y., Saito, M.A., Scott, P.M., Henderson, G.M., 2016. Rare earth elements (REEs) in the tropical South Atlantic and quantitative deconvolution of their non-conservative behavior. Geochim. Cosmochim. Acta 177, 217–237. https://doi.org/10.1016/j.gca.2016.01.018.

Zubkov, M.V., Sleigh, M.A., Burkill, P.H., Leakey, R.J.G., 2000. Picoplankton community structure on the Atlantic Meridional Transect: a comparison between seasons. Prog. Oceanogr. 45, 369–386. https://doi.org/10.1016/S0079-6611(00)00008-2.